Stability and breakup of confined threads

Stability and breakup of confined threads

P. J. A. Janssen,[a] H. E. H. Meijer,[a] and P. D. Anderson[a]
Materials Technology, Department of Mechanical Engineering, Eindhoven University of Technology, PO Box 513, 5600 MB Eindhoven, The Netherlands

(Received 2 October 2011; accepted 5 December 2011; published online 31 January 2012)

A boundary-integral method for periodic arrays of drops, threads or sheets between parallel walls is presented. The Green's functions take the form of a far-field Hele-Shaw description, which is used to generate periodic Green's functions for the parallel-wall configuration. The method is applied to study the effect of confinement on the breakup of threads. A comparison is made with classical Tomotika's theory and growth rates parallel and perpendicular to the walls are determined as a function of confinement ratio. Contrary to existing belief, we find that confined threads are not stable, but that the time for breakup increases with confinement and viscosity ratio, at least for threads whose diameter is smaller than the wallspacing. We also show the in-phase and out-of-phase breakup for an array of threads, as well as the stabilizing effect of shear flow. © *2012 American Institute of Physics*. [doi:10.1063/1.3677682]

I. INTRODUCTION

Microfluidic devices are often promoted as being able to generate a monodisperse drop distribution.[1,2] But besides drops, also morphologies such as threads and sheets exist in confined geometries, where at least one dimension is much larger than the wall spacing. In flow-focusing devices, it is possible to create long jets, but in general these eventually break up due to jetting or dripping.[3] The thread stability can be significantly increased by using specific geometries,[4] surfactants,[5,6] or visco-elastic fluids.[7] Another route to generate strings is by coalescence in a confined blend.[8] A rich collection of different morphologies found in sheared, confined blends is now known such as drops, squashed drops, pearl necklaces, and threads,[9–12] where the threads are actually stable, unlike threads in bulk flow.

The capillary instability of a thread has been known for a long time. For unconfined threads, pioneering work was conducted by Plateau[13] and Lord Rayleigh,[14] whose theory on the breakup of threads in air was later expanded and generalized by Tomotika for threads surrounded by viscous fluids in quiescent conditions[15] and in extensional flow.[16] Consider a thread with radius R_0 with a sinusoidal disturbance with amplitude α_0 and wavelength ω, as shown in Figure 1. Conservation of volume requires that the mean radius R of the thread changes with the amplitude as

$$R = \sqrt{R_0^2 - \frac{\alpha_0^2}{2}}. \tag{1}$$

Small-amplitude sinusoidal distortions on the thread interface will grow if growth results in a reduction of the surface area. For this, the wavelength ω of the distortion has to be greater than the critical value $2\pi R_0$. This is often reformulated as

$$X = \frac{2\pi R_0}{\omega} < 1, \tag{2}$$

with X the dimensionless wave number. Tomotika's theory states that in the initial small-deformation limit, the amplitude of the distortion α will then grow exponentially in time:

[a] http://www.mate.tue.nl.

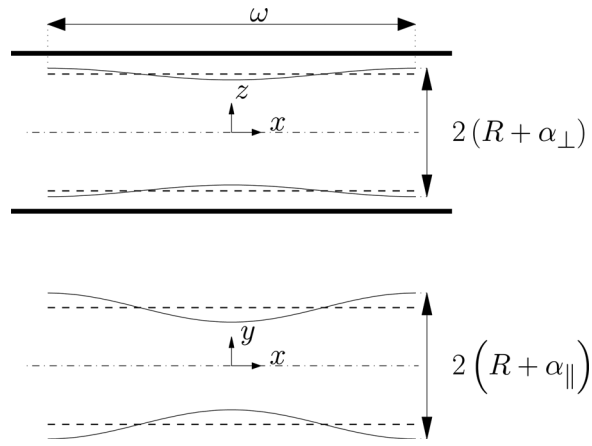

FIG. 1. Schematic representation of a confined thread with mean radius R and walls located at $z = \pm W$. On the thread sits a sinusoidal disturbance with wavelength ω and initial amplitude α_0. In time, the amplitude of the disturbance can vary parallel and perpendicular to the walls, denoted by $\alpha_\parallel$ and $\alpha_\perp$, respectively.

$$\alpha = \alpha_0 \exp(qt), \tag{3}$$

where the growth rate is given as

$$q = \frac{\sigma \Omega(X, \lambda)}{2\mu_0 R_0}, \tag{4}$$

where μ_0 is the viscosity of the matrix, σ is the interfacial tension, and λ denotes the viscosity ratio. The function Ω as function of X and λ can be found in Tomotika[15] (for $\lambda = 1$, Stone and Brenner[17] provide the same solution in an easier form). Reformulating Eq. (3) in dimensionless variables yields

$$\alpha = \alpha_0 \exp\left(\frac{\Omega(X, \lambda)}{2} t^*\right), \tag{5}$$

where t^* is time made dimensionless with $\sigma/R\mu$. For arbitrary viscosity ratio, there is a wave number X that grows the fastest and that is the dominating one for the breakup of the thread. Since the surface tension is the driving force for the growth rate of the distortion, the breakup of a thread can be used to measure interfacial tension, as done by Elemans *et al.*[18] An extensive review on the breakup of threads and jets has been written by Eggers.[19]

The behavior of multiple threads interacting with each other is also interesting. Elemans *et al.*[20] experimentally investigated the breakup of an array of threads. Knops *et al.*[21] later continued this work and conducted additional experiments, identifying different breakup phenomena. Depending on the distance between the threads, threads can either break up in-phase or out-of-phase; threads that are close together break up in-phase, and larger separations lead to out-of-phase breakup, where the critical distance is a function of the viscosity ratio. Analysis by Knops *et al.*[21] and Gunawan *et al.*[22] showed the critical distance to be about 3 thread radii for a viscosity ratio of unity, and with increasing the viscosity ratio, the critical separation distance increases. Hagedorn *et al.*[23] conducted several lattice-Boltzmann simulations for threads placed next to each other and noted: "For an inter-thread spacing less than or equal to 1.5 thread diameters, the threads tended to fuse at apparently random points… ." Although not described as such by these authors, this might also be considered as in-phase breakup, where the coarseness of the simulation technique prevents the ability to distinguish between touching and coalescing drops.

The influence of flow on morphology development is relevant for processing. Tomotika's result for extensional flow[16] was later expanded by Mikami *et al.*,[24] and even later by Khakhar and Ottino,[25] studying breakup of liquid threads with finite lengths in shear and extensional flows. Frischknecht[26] studied phase-separating blends in shear slow and focused on both the hydrodynamic Rayleigh instability, as well as the thermodynamic instability, and gave a critical capillary

number of 0.18 for $\lambda = 1$; Gunawan *et al.*[27] reported this to be 0.16 above which infinitely long equi-viscous threads are always stable in shear flow.

Considering confinement, Son *et al.*[28] used experiments, lattice-Boltzmann simulations, and a simple analytical calculation to investigate the stability of confined threads. Their main result is that confinement hinders growth of the local radius in the direction perpendicular to the walls, which leads to shapes with a non-axisymmetric cross section. This generates less driving force for the growth of the amplitude of the waves since the surface-volume ratio is less ideal compared to the case of circular cross sections. Also ribbons (threads where the primary axis of the cross section is much larger than the minor one due to "squashing" of the thread between the walls) formed by coalescence of drops are stable.[8] More lattice-Boltzmann simulations for threads in tubes and between parallel plates were conducted by Hagedorn *et al.*,[23] mainly focusing on the tube configuration, reporting various resulting drop shapes.

In this paper, a periodic algorithm is presented to study confined threads. First, some details concerning the boundary-integral formulation and the mesh generation algorithm are given. Next, the focus is on the growth of sinusoidal instabilities, and results are shown how confinement affects this growth perpendicular and parallel to the walls. Finally, the effect of multiple interacting threads is investigated, where the stabilizing influence of shear flow is also briefly discussed.

II. ALGORITHM FOR PERIODIC GREEN'S FUNCTIONS

Consider an infinitely long thread with radius R in creeping flow conditions between parallel walls. The walls are located at $z = \pm W$. The thread viscosity is given by μ_1, the matrix viscosity by μ_0, and the viscosity ratio is defined as $\lambda = \mu_1/\mu_0$. An interfacial tension σ acts between the thread and matrix. In this work, the interfacial tension is assumed to be constant, but without any restriction, the current model can be extended to include Marangoni stresses.

To non dimensionalize this problem, all length scales are scaled with R (in the case of small initial amplitudes, the difference between R and R_0 is negligible), pressure with σ/R, and time with $\sigma/R\mu_0$. In the presence of external flow fields, additional time scales enter the problem. For Couette shear flow, this time scale is the shear rate $\dot{\gamma}$; for pressure-driven flows, this is $U_{\max}/R$. The ratio between the time scales of the external flow and the capillary time scale is the capillary number Ca, which is defined for Couette flow as $\mathrm{Ca}_{\mathrm{Cou}} = R\dot{\gamma}\mu_0/\sigma$ and for pressure-driven flow as $\mathrm{Ca}_{\mathrm{Pois}} = U_{\max}\mu_0/\sigma$. The remaining parameter that characterizes the flow problem is the confinement ratio R/W.

The discontinuity in the normal stress across the interface is given by $\mathbf{f}$, which reads in non-dimensional form:

$$\mathbf{f}(\mathbf{x}) = 2\kappa(\mathbf{x})\mathbf{n}(\mathbf{x}), \tag{6}$$

with $\mathbf{n}$ the vector normal to the interface and κ the local mean curvature. The curvature is defined as $\kappa = \frac{1}{2}\nabla_s \cdot \mathbf{n}$, with ∇_s the surface gradient operator: $\nabla_s = (\mathbf{I} - \mathbf{nn}) \cdot \nabla$, where $\mathbf{I}$ is the unit tensor. Note that $\mathbf{f}$ in Eq. (6) only includes the capillary pressure, but can be extended to include van der Waals forces, density differences, or gradients in interfacial tension.[29,30]

To compute the velocity at any given point in the domain, a boundary-integral method[31,32] is used, where the velocity $\mathbf{u}$ at the pole $\mathbf{x}_0 = (x_0, y_0, z_0)$ is given by

$$\begin{aligned}(\lambda+1)\mathbf{u}(\mathbf{x}_0) = 2\mathrm{Ca}\mathbf{u}_\infty(\mathbf{x}_0) &- \frac{1}{4\pi}\int_S \mathbf{f}(\mathbf{x}) \cdot \mathbf{G}(\mathbf{x}, \mathbf{x}_0) dS(\mathbf{x}) \\ &- \frac{\lambda - 1}{4\pi}\int_S \mathbf{u}(\mathbf{x}) \cdot \mathbf{T}(\mathbf{x}, \mathbf{x}_0) \cdot \mathbf{n}(\mathbf{x}) dS(\mathbf{x}),\end{aligned} \tag{7}$$

where the integration is over all thread surfaces S. Furthermore, $\mathbf{u}_\infty$ is the prescribed velocity field. For the parallel wall configuration, the only relevant flows are Couette flow $\mathbf{u}_\infty = (z, 0, 0)$ and Poiseuille flow $\mathbf{u}_\infty = \left(\frac{(W-z)(W+z)}{W^2}, 0, 0\right)$. Finally, $\mathbf{G}$ and $\mathbf{T}$ represent the Green's functions for velocity and stress, respectively, associated with the flow due to a point force, also known as the single- and double-layer potential, or the Stokeslet and the stresslet.

The requirement that the velocity components should vanish at the wall is obeyed by modifying the Green's functions **G** and **T** to include the free-space result and a part with the additional contributions due to the presence of the walls:

$$\mathbf{G} = \mathbf{G}^{\infty} + \mathbf{G}^{2W}; \quad \mathbf{T} = \mathbf{T}^{\infty} + \mathbf{T}^{2W}, \tag{8}$$

where the free-space parts are given by

$$\mathbf{G}^{\infty}(\mathbf{x}, \mathbf{x_0}) = \frac{\mathbf{I}}{|\hat{\mathbf{x}}|} + \frac{\hat{\mathbf{x}}\hat{\mathbf{x}}}{|\hat{\mathbf{x}}|^3}, \quad \mathbf{T}^{\infty}(\mathbf{x}, \mathbf{x_0}) = -6\frac{\hat{\mathbf{x}}\hat{\mathbf{x}}\hat{\mathbf{x}}}{|\hat{\mathbf{x}}|^5}, \tag{9}$$

with $\hat{\mathbf{x}} = \mathbf{x} - \mathbf{x}_0$, and $\mathbf{x} = (x,y,z)$ is the field point. We can also define a pressure vector **Q** associated with the pressure field generated by a point force. Similarly, **Q** has a free-space and a wall correction as well. The wall corrections consist of Fourier-Bessel integrals[33] of the form

$$G_{zz}^{2W} = \int_0^{\infty} J_0(qs) t_{1nn}(q, z, z_0) dq, \tag{10}$$

with J_0 a Bessel function of the 1st kind of 0th order, $s = \sqrt{\hat{x}^2 + \hat{y}^2}$, and t_{1nn} a function found in Jones.[33] Exact details of the form of these functions and how to evaluate the integrals fast can be found elsewhere.[34,35]

One important characteristic of these Green's functions is that they approach a Hele-Shaw form at high values of s. At high s, **G** is given by[36,37]

$$\mathbf{G} = \mathbf{G}^{\mathrm{HS}} + O\left(\mathrm{e}^{-s/2W}\right), \tag{11}$$

where the Hele-Shaw form is defined as

$$\mathbf{G}^{\mathrm{HS}} = -\frac{1}{2}\mu^{-1}(W - z)(W + z)\nabla \mathbf{Q}^{HS}, \tag{12}$$

with

$$\mathbf{Q}^{\mathrm{HS}} = -\frac{3}{8W^3}\pi^{-1}(W - z_0)(W + z_0)\nabla\psi(\hat{x}, \hat{y}), \tag{13}$$

and $\psi = -\ln(s)$ is the solution of the two-dimensional Poisson equation:

$$\nabla^2\psi(\hat{x}, \hat{y}) = -2\pi\delta(\hat{x}, \hat{y}). \tag{14}$$

In other words, we can define a kernel $\boldsymbol{\delta}\mathbf{G}$:

$$\delta\mathbf{G} = \mathbf{G}^{\infty} + \mathbf{G}^{2W} - \mathbf{G}^{\mathrm{HS}}, \tag{15}$$

that decays exponentially to **0**, the further one is away from the pole. The physical interpretation of the Hele-Shaw form is that all velocities in z direction decay exponentially, and forces applied in the z direction have an exponential decaying contribution to the velocity field. Finally, the double-layer potential **T** is defined as[32]

$$T_{ijk} = -\delta_{ik}Q_j(\mathbf{x}, \mathbf{x}_0) + \frac{\partial G_{ij}}{\partial x_k}(\mathbf{x}, \mathbf{x}_0) + \frac{\partial G_{kj}}{\partial x_i}(\mathbf{x}, \mathbf{x}_0). \tag{16}$$

To study periodic structures like long threads and sheets, a periodic domain with a length of L_x in the x-direction and L_y in the y-direction is considered (see Figure 2). As mentioned before, in the third dimension, the walls are placed at $z = \pm W$. For this, a periodic version of the Green's functions **G** and **T** needs to be implemented. Various ways to handle three-dimensional free-space kernels exist and have been used in the past to study blends.[38–41] A straightforward technique is to make an Ewald summation over **G** and **T.**[42] However, Ewald summations, or similar techniques, do not exist for the Fourier-Bessel integrals.

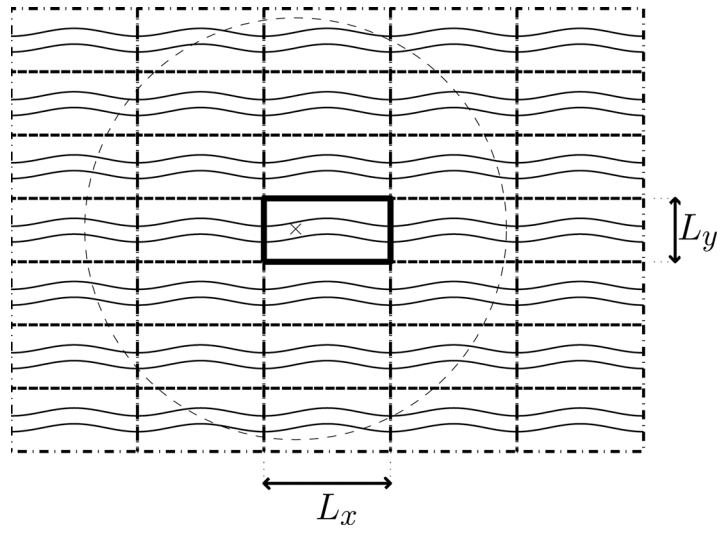

FIG. 2. The computational domain for periodic structures. The rectangle with the bold lines in the middle is the original domain with a periodic structure inside it, and several layers of periodic images are shown around it. The cross represents a pole location which is needed for evaluation. The term $\delta\mathbf{G}$ only has to be evaluated in the dotted circle with radius s_c around the cross.

To properly evaluate periodic Green's functions between parallel walls, an algorithm similar as proposed by Blawzdziewicz and Wajnryb[43] is used here. The basic idea is to subtract the Hele-Shaw formulation from the full Green's functions in a limited number of points and then to add the Hele-Shaw formulation efficiently summed over the whole domain.

To this end, a number of periodic images of the original computational domain are made (see Figure 2). For each pole-field point combination, $\boldsymbol{\delta}\mathbf{G}$ is summed over the original domain and all the periodic images of the field point. From Eq. (11), it is seen that $\boldsymbol{\delta}\mathbf{G}$ exponentially decays to $\mathbf{0}$, so the number of periodic images that needs to be included is limited. A circle around $\mathbf{x}_0$ with radius s_c can be now be defined, outside which $\boldsymbol{\delta}\mathbf{G}$ is practically $\mathbf{0}$, and does not have to be evaluated. Depending on the choice of L_x, L_y, and W, only a handful of layers of periodic images are required. In fact, the number of layers multiplied with L_x or L_y has to be at least s_c, but more layers are not required,

$$N_x L_x \geq s_c, N_y L_y \geq s_c, \tag{17}$$

where N_x and N_y are the number of periodic images in the x and y directions, respectively. The cut-off parameter s_c is set to $5W$ in this study, which proved to be sufficiently large for a properly decayed $\delta\mathbf{G}$ and $\delta\mathbf{T}$.

As $\mathbf{G}^{\mathrm{HS}}$ is subtracted, it has to be added again, but now summed over the whole domain. This term is the periodic version of the Hele-Shaw kernel: $\mathbf{G}^{\mathrm{HS}}_{\mathrm{per}}$, which leads to following formulation of the periodic Green's function $\mathbf{G}_{\mathrm{per}}$:

$$\mathbf{G}_{\mathrm{per}} = \sum_{\mathbf{l}} \delta\mathbf{G}(\mathbf{x} + \mathbf{l}, \mathbf{x}_0) + \mathbf{G}^{\mathrm{HS}}_{\mathrm{per}}, \tag{18}$$

where $\mathbf{l}$ is a two-dimensional vector, which components are integer multiples of L_x and L_y, respectively and which range from $-N_x$ to N_x for the x component and from $-N_y$ to N_y for the y component. What remains to be defined is an expression for $\mathbf{G}^{\mathrm{HS}}_{\mathrm{per}}$. This term is identical to $\mathbf{G}^{\mathrm{HS}}$ (see Eq. (12)), except that ψ in Eq. (13) is replaced with ψ_{per}, the solution of the periodic Poisson equation:

$$\nabla^2 \psi_{\mathrm{per}}(\hat{x}, \hat{y}) = -2\pi \left[\sum_{\mathbf{l}} \delta(\hat{\mathbf{x}}_2 + \mathbf{l}_2) - \left(L_x L_y\right)^{-1} \right]. \tag{19}$$

Here, $\mathbf{l}$ is the same two-dimensional vector as mentioned above, but now ranges from $-\infty$ to $+\infty$, and $\hat{\mathbf{x}}_2$ is a two-dimensional vector consisting of $\hat{x}$ and $\hat{y}$.

Various algorithms exist to efficiently compute ψ_{per};[44–46] here, the one proposed by Tyagi[47,48] is used

$$\psi_{\text{per}} = \sum_{m'=-\infty}^{\infty} L\left(\frac{\hat{x}}{L_x}, \frac{|\hat{y}+mL_y|}{L_x}\right) + L\left(\frac{\hat{x}}{L_x}, \frac{\hat{y}}{L_x}\right) + \frac{2\pi}{12L_x}\left(1 - 6\frac{|\hat{y}|}{L_y} + 6\left(\frac{\hat{y}}{L_y}\right)^2\right), \tag{20}$$

where the prime indicates that $m=0$ is to be skipped, and the function L is defined as

$$L(x,y) = -\frac{1}{2}\ln(1 - 2\exp[-2\pi y]\cos[2\pi x] + \exp[-4\pi y]). \tag{21}$$

Derivatives up to second (third) order in x and y are needed to evaluate $\mathbf{G}(\mathbf{T})$, but these are straightforward to derive and not shown here. Furthermore, depending on pole and field point location, $\hat{x}$ and $\hat{y}$ have to be modified such that

$$-L_x/2 < \hat{x} \leq L_x/2, \quad -L_y/2 < \hat{y} \leq L_y/2, \tag{22}$$

which can be achieved by taking the proper modulus. To evaluate ψ_{per} at $s=0$, expressions for the self interaction are used, which can be found in the papers of Tyagi.[47,48] Blawzdziewicz and Wajnryb[43] provide expressions for $\mathbf{G}_{\text{per}}^{\text{HS}}$ and $\mathbf{Q}_{\text{per}}^{\text{HS}}$ based on Ewald summations. The non-periodic components of the Green's function have singularities at $\mathbf{x}=\mathbf{x}_0$ for the free-space part and at the wall for the wall corrections. The former can be tackled by using singularity subtraction,[32] which is used here, as well as non-singular contour integration;[30] the latter situation does not occur in our case, as the matrix fluids fully wets the walls.

The choice of L_x and L_y determines the morphology. For example, with a large value of L_y and a small value of L_x, one can study an isolated train of drops or other isolated structures which are only periodic in the x-direction. However, for the threads with sinusoidal distortions as studied in this paper, L_x cannot be chosen freely and depends on the wavelength of the distortion. The number of layers of periodic images has to be adjusted properly, of course. The current method has no ability to modify the wavelength during a simulation.

To handle non-unit viscosity ratios, an iterative procedure was used to solve for $\mathbf{u}$ in Eq. (7). Uniform expansion and rigid body modes were purged from the solution spectrum to speed up the convergence.[32,49]

III. MESH GENERATION

The generation of the mesh for threads differs from that of spherical drops. The basis of the mesh is a tube with length L_x and radius R_0, and the only free parameter to define the coarseness is n, which defines the number of rows of nodes in the x direction. This immediately gives Δx, the separation between the rows. As equilateral triangles are desired for a more accurate curvature calculation, the number of nodes in circumferential direction n_{circ} is then given by

$$n_{\text{circ}} = \frac{\pi R_0}{\tan(\pi/6)\Delta x}, \tag{23}$$

rounded to the nearest integer value. The nodes in one row are then simply generated by projecting them on a unit circle with a distance between each node of $\Delta\theta = \frac{2\pi}{n_{\text{circ}}}$ rad. Each subsequent row of nodes is shifted with $\Delta\theta/2$ over the unit circle to generate a mesh with equilateral triangles (see Figure 3). All nodes have a connectivity number 6, which is optimal. Alternatively, the number of nodes in circumferential direction can be fixed, and then the number of nodes in the length can be derived.

Due to the periodicity of the mesh, and due to the fact that the first and last row of nodes lack neighboring nodes, two rows of "ghost nodes" are introduced. These are nodes with identical properties to their real counterparts on the other side of the mesh, but their x location is shifted with $\pm L_x$. Furthermore, the ghost nodes are connected to the nodes on the edge of the domain, so that the curvature and normal vector can be computed here. The ghost nodes on either side of the

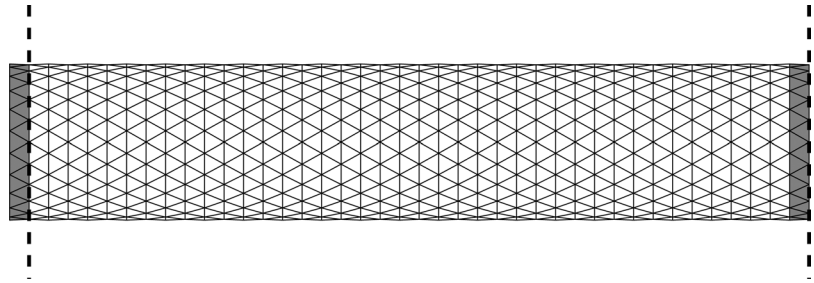

FIG. 3. Mesh generated to study infinitely long threads with the number of rows of nodes in the x direction $n = 40$ (top view). The boundaries of the periodic domain in the x direction are indicated with the dashed line. The light-colored elements are formed with only "real" nodes, whereas the dark-colored ones are formed with real nodes on the edge and "ghost nodes". Notice that the row of ghost nodes on the right is on the edge of the domain, as the periodicity makes it an exact mirror image of the first row of real nodes on the other side of the domain, while the row of ghost nodes on the left is outside the domain. Not shown are the elements that connect both rows of ghost nodes, to generate a closed, highly-distorted donut-shaped mesh.

domain are also connected to each other via extremely distorted elements. Although these elements are not taken into account in the boundary-integral equations, they ensure that the mesh is closed, which provides the ability to conduct various checks on the number of nodes, sides, elements, and connectivity numbers. We also ensure that during the simulation, the nodes which lay right on the edge of the domain (at $x = -L_x/2$) do not leave the edge ($u_x = 0$), but can still move on it. This ensures that the mesh remains in good shape and nodes on the edge of the domain do not get flipped to the other side.

Finally, we note that any mesh can be used in the periodic domain, including fully closed surfaces such as drops, as well two surfaces that represent a sheet of a liquid in the matrix fluid. Of course, sheets are stable versus capillary instabilities, as there is no surface area decrease with increasing growth of disturbances, but the configuration could be relevant for other problems.

IV. RESULTS

In this section, several results are presented, with the main focus on the comparison with published results, especially for unconfined threads, and subsequently show the influence of the presence of walls. Comparison of the boundary-integral method results with Tomotika's theory serves as a validation of the model.

A. Initial growth speed

First, the stability of a confined thread with a unit viscosity ratio is investigated. Son *et al.*[28] reported different growth rates parallel and perpendicular to the walls for different confinement ratios. Here, this is investigated in a more systematic way. Five confinement ratios are considered, and for each of them, several values of the wave number X are investigated. The size of the periodic domain in the x direction is adjusted to the wavelength and $L_y = 50$. The simulations have to run for a short time span, since only the initial growth rate is considered. The results are shown in Figure 4. For the unconfined case ($R/W = 0.1$), an excellent agreement with Tomotika's theory is obtained, and only a minor difference between the parallel and perpendicular growth rate is found. Increasing the confinement ratio results in a decrease in the growth rate for both the parallel and perpendicular direction, but the effect is by far the strongest for the perpendicular case, where it is already significantly reduced for a relatively low confinement ratio of $R/W = 0.3$ and becoming virtually 0 for $R/W = 0.9$. This makes sense, as the walls hinder the growth in this direction. The parallel growth speed rates show only a modest change.

Next, the influence of the viscosity ratio is shown. In Figure 5, the results for a viscosity ratio of $\lambda = 0.2$ are shown. Similar trends as in the case of unit viscosity ratio are observed: the walls decrease the growth speed of the amplitude, but considerably more in the direction perpendicular to the walls. Results for $\lambda = 4$ are shown in Figure 6. The absolute value of the growth speed is lower as expected, and once again, a significant reduction in the growth speed due to the walls. An

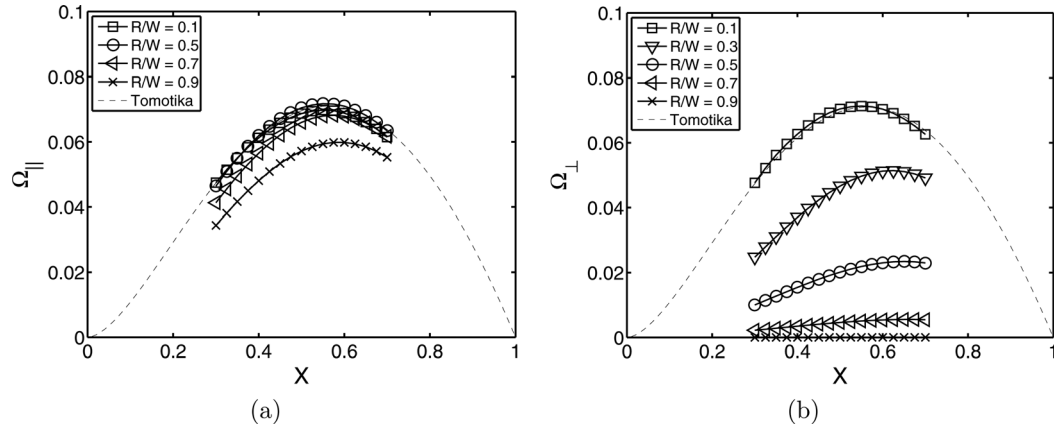

FIG. 4. Initial growth speed factor Ω of the disturbance as function of the wave number X: (a) parallel to the walls (b) perpendicular.

interesting observation is the shift that the wave number with maximum growth rate makes. For $\lambda = 1$ and $\lambda = 4$, it shifts to larger values for the parallel and perpendicular amplitudes, but the wave number with maximum growth rate moves to lower values of X for $\lambda = 0.2$. In the experimental study of Son *et al.*,[28] it was reported that X shifts to a lower value with increasing confinement ratio for a viscosity ratio $\lambda = 0.25$. More quantitative data for this shift in wavenumber are shown in Figure 7, where the wavenumber with maximum growth rate is shown as a function of the confinement ratios for various viscosity ratios λ. For $\lambda < 0.4$, $X_{\max}$ shifts to lower values, while for $\lambda > 0.4$, it shifts to higher values. At $\lambda = 0.4$, there is no notable change. In all cases, the minimal wavelength needed for the growth of an instability remains unchanged ($X = 1$), which is as expected, since that criterion comes from the fact that only for waves with a wavelength that is large enough, the surface area reduces with growing amplitude, regardless of the actual growth rate.

B. Breakup

In Sec. IV A, we have seen that the effect of confinement is a decrease in the magnitude of the growth rate independent of viscosity ratio. Next, the influence of the confinement on growth of the instability until the moment of breakup is shown. The initial disturbance has a wavelength $\omega = 10$ (or $X = 0.62$, which is fairly close to the maximum wave number for all confinement ratios) and initial amplitude $\alpha_0 = 0.01$. The periodic domain is adjusted to the wavelength and given by $L_x = 10$, $L_y = 20$, and the wall separation is systematically varied. For various confinement ratios, the evolution in time of the radius parallel and perpendicular to the wall, as well as for radius of the neck, both parallel and perpendicular, is shown in Figure 8; the breakup time as

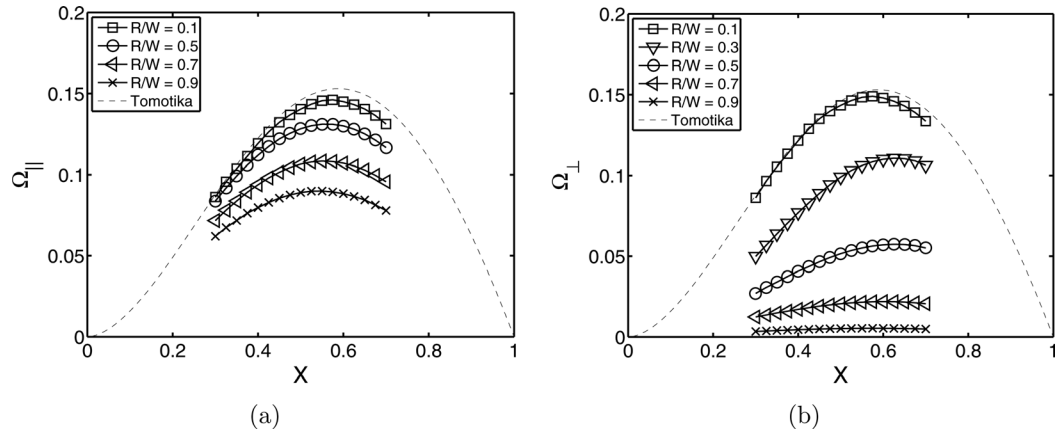

FIG. 5. As Fig. 4, but with $\lambda = 0.2$.

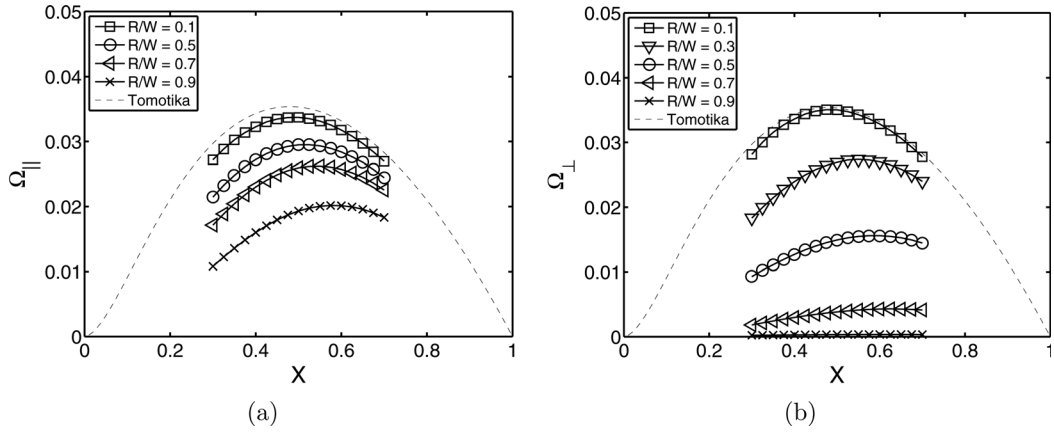

FIG. 6. As Fig. 4, but with $\lambda = 4$.

function of the confinement ratio is shown in Figure 9. Breakup is found for all $R/W \leq 0.9$ and for the three different viscosity ratios studied, $\lambda = 0.25$, 1, and 4. In Figure 8, four lines are plotted for each confinement ratio: R_{par} the radius in parallel direction, R_{per} the radius in perpendicular direction, and $R_{\text{neck,max}}$ and $R_{\text{neck,min}}$ which denote the maximum and minimum radii of the neck. For all viscosity ratios, similar trends are observed. For larger confinement ratios, the difference between R_{par} and R_{per} becomes larger as a function of time, indicating the cross section of the threads is no longer circular. Similarly, the neck also loses its round cross section, especially for the higher confinement and viscosity ratios.

Not directly visible from the graph is that for the unconfined case, the disturbance initially remains sinusoidal: the amplitude of the disturbance for the neck as well as for the thicker part remains identical. For most confinement and viscosity ratio, we find that the amplitude keeps growing exponentially in time, right until breakup, although the growth rate itself can differ. The only significant deviations are seen for $R/W = 0.9$, where the deviation from exponential behavior starts earlier: in particular, the growth speed perpendicular to the walls slows down significantly in time.

In all situations, breakup occurs after some time and the breakup time increases significantly compared with $R/W = 0.1$, roughly a factor 3.5 at $R/W = 0.9$ as seen in Figure 9(b). This might explain the reporting of *apparently* stable threads in confinements,[8] where in reality, the breakup time is much larger than the experimental time scale. So, threads could be considered kinetically stable, although they might not be thermodynamically. In the analysis of Son *et al.*,[28] it was argued that confined threads are stable between walls, because the non-axisymmetric growth of the thread no longer leads to a decrease in surface area for all wavelengths and forces an increase

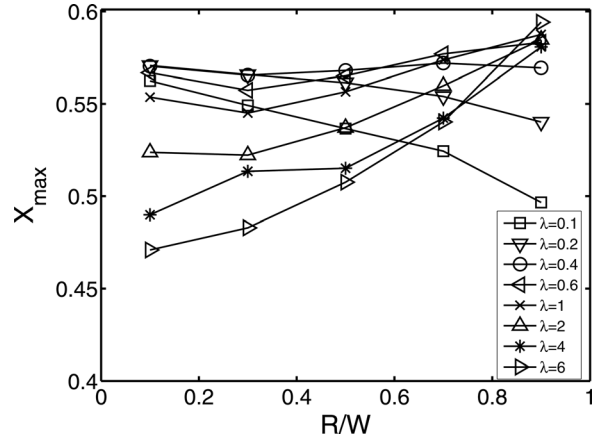

FIG. 7. The wavenumber with maximum growth rate in parallel direction as function of R/W for multiple viscosity ratios.

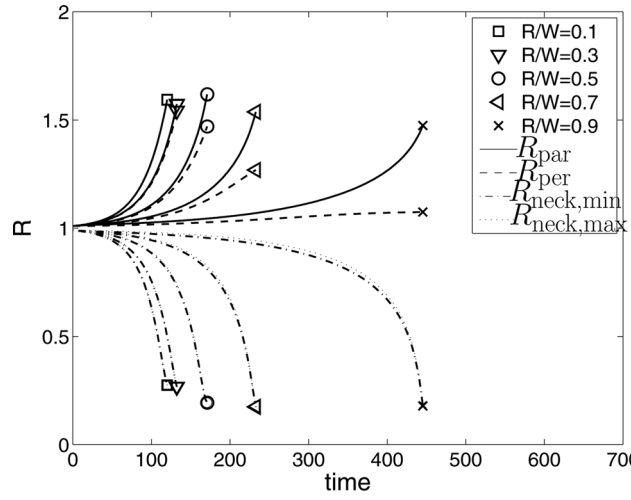

(a)

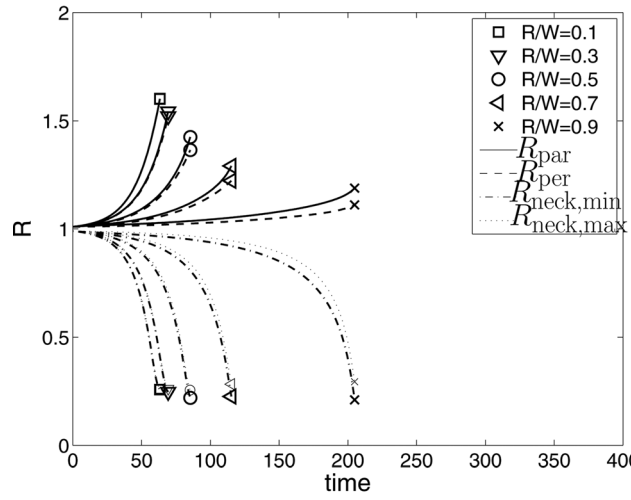

(b)

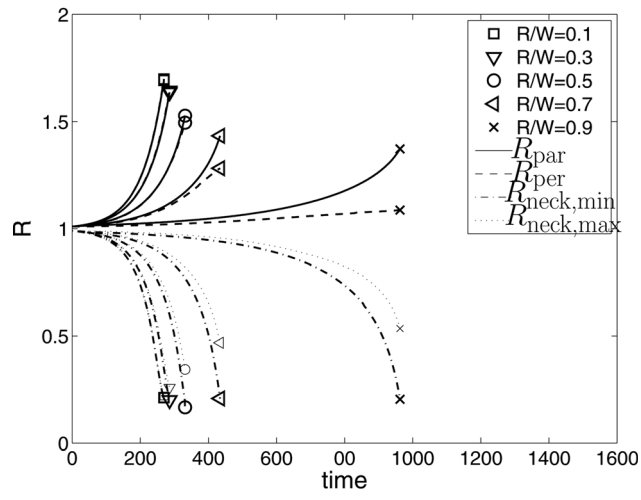

(c)

FIG. 8. Evolution of the major radii (a) $\lambda = 1$, (b) $\lambda = 0.25$, and (c) $\lambda = 4$. The initial disturbance was characterized with $\omega = 10$ and $\alpha_0 = 0.01$.

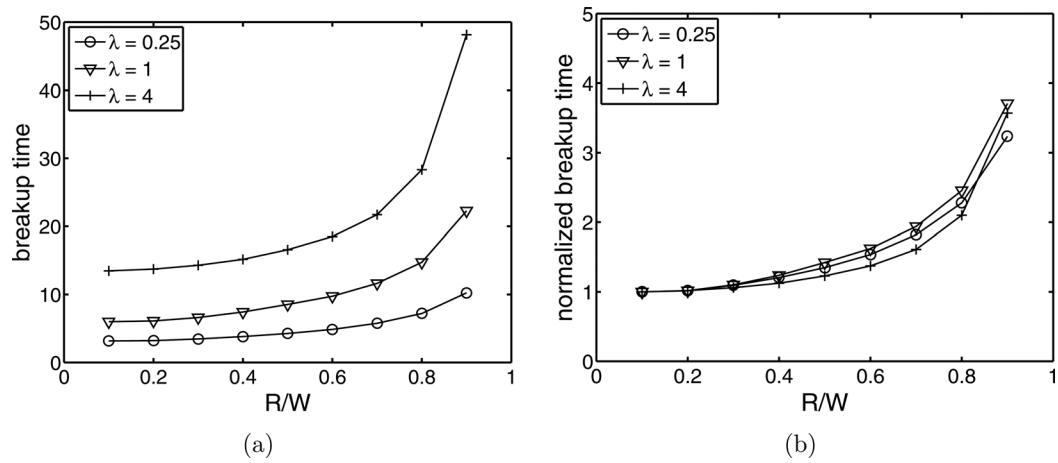

FIG. 9. Breakup times as a function of confinement ratio for all viscosity ratios (a) Breakup times (b) Breakup times normalized with the breakup time at $R/W = 0.1$.

in the wavelength, which diverges to infinity. For the confinement ratio we have explored here, the results are in disagreement with this, as growth of the instability and reduction of surface area are observed for all confinement ratios. The analysis presented by Son *et al.*[28] might be a little too simple to capture the dynamics of the whole thread. In particular, they considered an elliptic cross section with a disturbance that remains sinusoidal, regardless of the amplitude.

Over-confined threads ($R/W > 1$) are stable versus small-amplitude disturbances due to the fact that no reduction in surface area can be achieved. In real systems, these threads are formed by the coalescence of "squashed drops." To model this, the choice of the initial conditions of the thread is not straightforward. The thread dimensions in the z direction need to be reduced to fit the thread between the walls and increased the y direction to obtain the same volume. The question is then what to do with the amplitudal disturbance. Although of interest, this is beyond the scope of this paper. For threads with $0.9 < R/W < 1$ by extrapolation, we still expect breakup, but with a breakup time diverging to infinity.

The influence of the initial amplitude of the disturbance on the breakup time is shown in Figure 10. Once again, a wavelength of 10 was chosen, and the domain in y large enough to consider the threads as isolated ($L_y > 20$). The viscosity ratio was 1. The results are as expected: larger initial amplitudes give a shorter breakup time, and as shown before: larger confinement ratios give a higher breakup time. The logarithmic behavior of the breakup time as function of α_0 is exactly

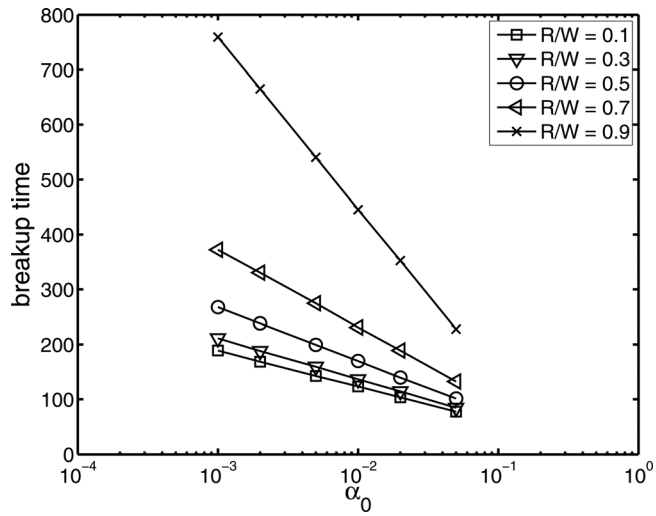

FIG. 10. The breakup time as function of the initial amplitude of the distortion for various confinement ratios.

TABLE I. Parameters to fit Fig. 10 with Eq. (24).

R/W	0.1	0.3	0.5	0.7	0.9
A	−7.28	−12.15	−26.51	−51.34	−179.52
B	−28.43	−32.29	−42.57	−61.39	−135.89

as expected; a simple scaling argument gives the breakup time as the time when the amplitude has reached a value of R. As the amplitude increase exponential in time, the breakup time has a logarithmic dependence. The results cannot be directly extrapolated to larger amplitudes, because for larger amplitudes, the thread would not fit between the walls without distorting the initial shape. The graphs in Figure 10 have been fitted to the following equation:

$$t_{\text{break}} = A + B \ln \alpha_0. \tag{24}$$

The values for the fit can be found in Table I. From this, we extrapolate a hypothetical cross-over point, where all confinement ratios have the same breakup time. This cross-over point lies at an initial amplitude of about $\alpha_0 = 0.25$. This value is so large that we conclude that confinement in all cases will lead to an increase in the breakup time.

The values for the breakup time, we find here compare favorable to the experimental results of Son *et al.*[28] For their unconfined system with $\lambda = 0.25$ and $R/W \approx 0.1$, they report a breakup time of about 700 s. With system parameters of $\sigma = 5.7$ mN/m, $\mu_0 = 1200$ Pa.s, and $R_0 = 63\,\mu$m, we convert our dimensionless breakup time of 63 into a corresponding value of about 800 s. For their confined system with $R/W = 0.7$, we find about 1600 s for our simulation versus their 1250 s. The difference can easily be explained by the unknown magnitude of the initial amplitude, which is next to impossible to measure with optical techniques, and a different in wavelength, which here is fixed at 10, but in reality will be the one with the largest growth rate.

C. Effect of Couette shear flow on stability of threads

Apart from confinement, Couette shear flow can also slow or even halt the growth of perturbations. To illustrate that, we show several images to show the influence of shear flow. Those are presented in Figure 11, one for $\text{Ca} = 0.05$, which is found to break up and thus below the critical

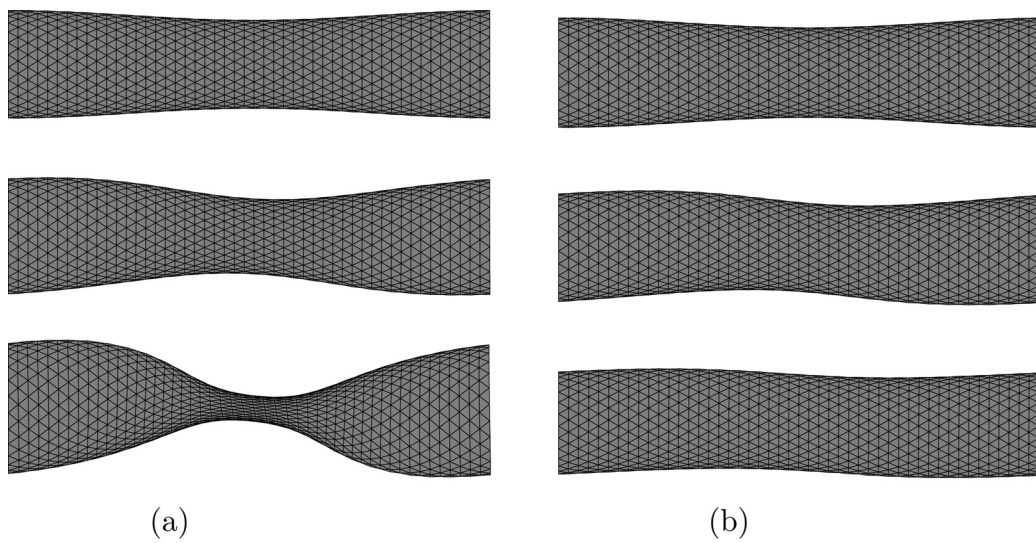

FIG. 11. Images of the thread shape taken at dimensionless times $t = 0$, $t = 40$, and $t = 80$ for a thread with $\omega = 10$, $R/W = 0.5$, $\alpha_0 = 0.1$, and (a) $\text{Ca} = 0.05$ (b) $\text{Ca} = 0.1$. The periodic domain was given by $L_x = 10$ and $L_y = 10$, and the coarseness of the mesh by $n = 50$, the number of nodes in the x direction.

capillary number, and one for $\mathrm{Ca} = 0.1$, which is supercritical and thus stable (in additional simulations, the critical capillary number was found to be 0.075).

A detailed study of the critical capillary number as function of all the parameters is beyond the scope of this study, but we want to establish how close our simulations are to other estimates. The reported value of 0.164 by Gunawan *et al.*[27] and 0.18 by Frischknecht[26] overestimate the critical value we find here (0.075) by a factor of 2 to 2.5. However, both studies do not take into account the initial amplitude of the disturbance α_0. A larger initial amplitude will give a larger $\mathrm{Ca}_{\mathrm{crit.}}$

Next, a simple scaling argument is presented to predict the critical capillary number above which threads are stable in Couette flow. As long as the shear flow can convect waves over a distance $\omega/4$ in a time shorter than it would take for the thread to break, the thread is stabilized. In that configuration, a minimal surface area is achieved by reducing the amplitude of the disturbance. To get an estimate of $\mathrm{Ca}_{\mathrm{crit,}}$ we need two time scales: (1) the breakup time, which according to Tomotika's theory is

$$t_{\mathrm{break}}\dot{\gamma} = \frac{2\mathrm{Ca}}{\Omega(X,\lambda)} \ln\left(\sqrt{\frac{2}{3}}\frac{R_0}{\alpha_0}\right), \tag{25}$$

and (2) the time it takes to convect waves

$$t_{\mathrm{convect}}\dot{\gamma} = \frac{\omega}{4R_0} = \frac{\pi}{2X}, \tag{26}$$

which gives a critical capillary number of

$$\mathrm{Ca}_{\mathrm{crit}} = \frac{\pi\Omega(X,\lambda)}{4X\ln\left(\sqrt{2/3}R/\alpha_0\right)}, \tag{27}$$

above which the thread is stable. The factor $\sqrt{\frac{2}{3}}$ originates from equaling the amplitude to the mean thread radius, which would give a neck radius of 0.[50] This estimate for the critical capillary number is likely to underestimate the true value, since the breakup of the thread is unavoidable even if the neck radius is not completely zero yet, and the growth rate of the distortion actually increases as the neck gets thinner.

A detailed study of the critical capillary number as function of all the parameters in Eq. (27) is beyond the scope of this paper, and only several images to show the influence of shear flow are presented in Figure 11, one for $\mathrm{Ca} = 0.05$, which is found to break up and thus below the critical capillary number, and one for $\mathrm{Ca} = 0.1$, which is supercritical and thus stable (in additional simulations, the critical capillary number was found to be 0.075).

Inserting values for an unconfined thread in Eq. (27) gives $\mathrm{Ca}_{\mathrm{crit}} = 0.0197$, which is an underestimation of about a factor of 4. A slightly different estimate can be made by taking the breakup time as shown in Figure 9, which is 8.55 for $\mathrm{Ca} = 0.05$ there. As the breakup time is linear in the capillary number and the convection time is $\omega/4 = 2.5$, this would give $\mathrm{Ca}_{\mathrm{crit}} = 0.0146$, which is even even lower. On the other hand, the reported value of 0.164 by Gunawan *et al.*[27] and 0.18 by Frischknecht[26] overestimate the critical value we find here. All in all, we conclude that Eq. (27) gives a reasonable estimate of $\mathrm{Ca}_{\mathrm{crit,}}$ but is by no means exact.

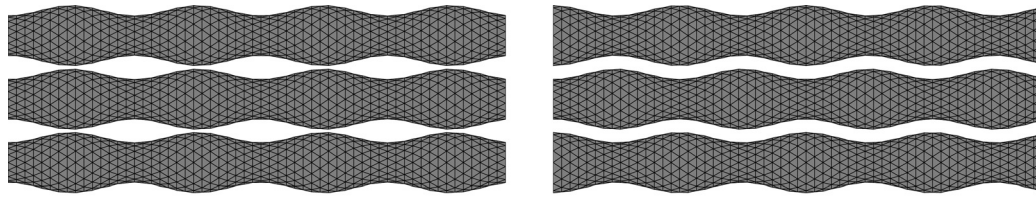

FIG. 12. The initial configuration to study the growth rate of (a) in- and (b) out-of-phase breakup behavior. The amplitude is enlarged and the wavelength reduced from the actual simulation.

D. Array of threads

In the previous sections of this paper, only the dynamics of a single thread was studied. Following a similar approach now an array of threads is considered. First, an attempt is made to reproduce the in-phase and out-of-phase breakup behavior, by placing three threads next to each

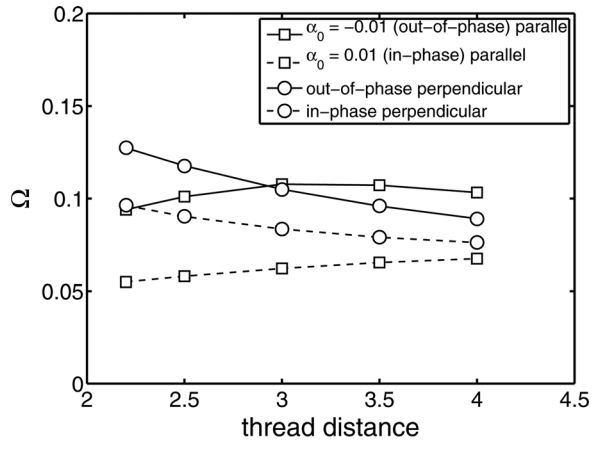

(a)

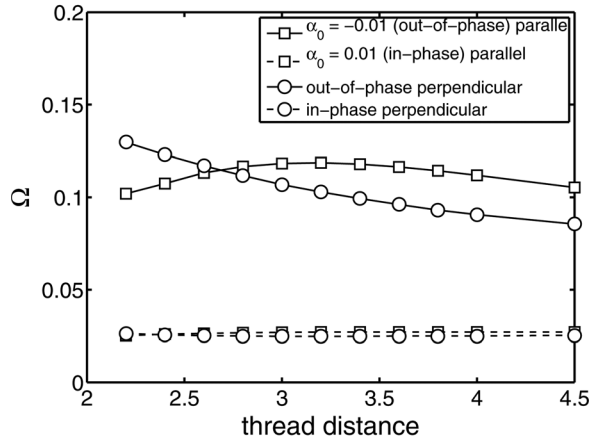

(b)

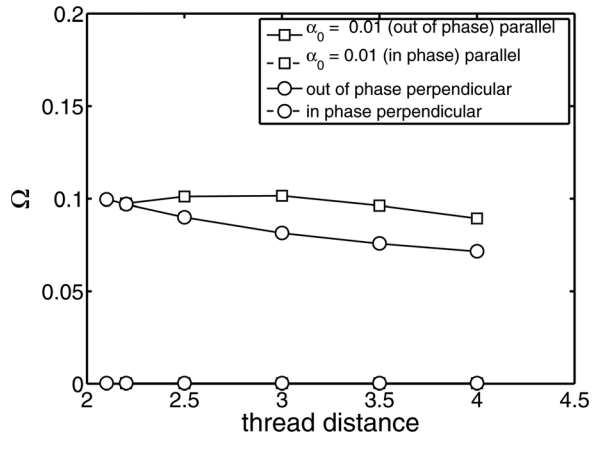

(c)

FIG. 13. The initial growth rate of a sinusoidal disturbance on a thread, laying in between two other threads as function of the thread separation for: (a) $R/W = 0.1$, (b) $R/W = 0.5$, (c) $R/W = 0.9$. The growth rates are plotted for in-phase and out-of-phase disturbances and well as parallel and perpendicular to the walls.

other, where similar as for the single thread, the initial growth rate again is considered. One thread (the middle one in case of three threads) is given a small-amplitude sinusoidal disturbance. On the neighboring threads, also a disturbance is placed, with either an identical (which leads to in-phase behavior), or one with the negative amplitude (resulting in out-of-phase behavior). Both situations are, albeit exaggerated, shown in Figure 12. The thread separation is varied, and the initial growth rate Ω for both situations is computed. The situation with the largest growth speed at a given thread separation is the most likely to occur and will, therefore, give the breakup behavior. If, instead of two threads next to each other, we consider two, but match L_y to be twice the distance between the threads to generate an infinitely large array, we find very similar growth rates. This indicates that the growth speed is dominated by the directly neighboring threads. The second configuration is more expensive to compute, because more periodic images in y directions have to be taken. Therefore, the results shown below are for the three-thread configuration.

Figure 13 shows the results for a configuration of three threads for three different confinement ratios, i.e., $R/W = 0.1$, 0.5, and 0.9. The middle thread has a disturbance with $\omega = 10$ and $\alpha_0 = 0.01$. The two threads on either side both have the same disturbance, but the amplitude is either 0.01 (in-phase) or -0.01 (out-of-phase). The thread separation is varied, and the growth rate for the in-phase as well as the out-of-phase initial condition is plotted as function of the separation.

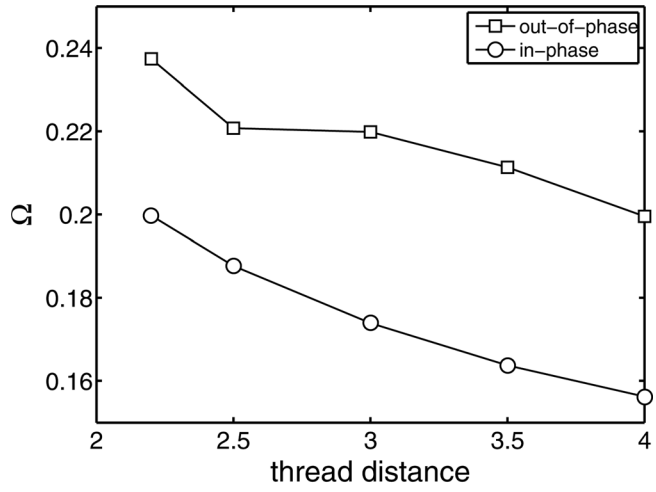

(a)

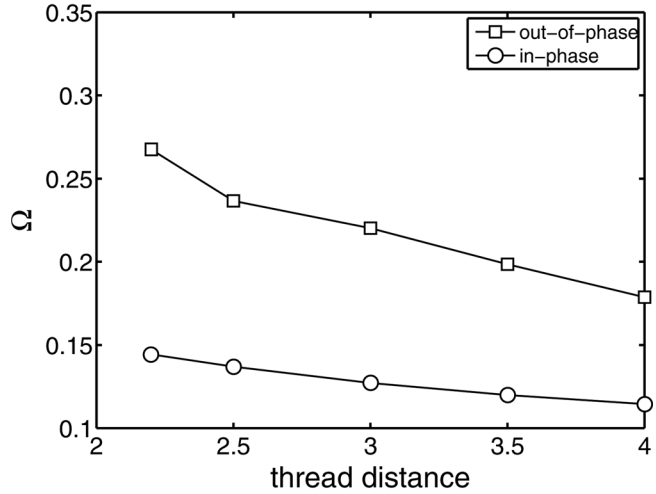

(b)

FIG. 14. As Fig. 13 for $\lambda = 0.25$ with: (a) $R/W = 0.1$, (b) $R/W = 0.9$, and only the parallel growth speeds.

Similar results as those obtained by Gunawan *et al.*[22] are found: for small separations, the in-phase configuration has the largest growth rate, and for large separations, and the out-of-phase behavior. The case for $R/W = 0.1$ can be considered the unconfined situation. For this, Gunawan *et al.*[22] found a critical thread distance of 3.14, which they suspected to be π exactly. The current results show a critical separation just below 3. Note that due to the discrete nature of the boundary-integral method obtaining growth rates is non exact, which might explain this minor difference. Furthermore, a confinement ratio of $R/W = 0.1$ is small, but non-zero and it still might have an influence. The current method is also periodic in y direction, although once this influence is small, as we find that the neighboring threads determine to a large extent the growth rates. When investigating different confinement ratios (0.5 and 0.9), it is obvious that with increasing confinement ratio, the critical separations shifts to smaller thread separations, as observed in Figures 13(b) and 13(c).

For $\lambda = 0.25$ and 4, results are shown in Figures 14 and 15, respectively. No cross-over distance is not found in Figure 14 for $\lambda = 0.25$, so we expect no in-phase breakup. This is consistent with experiments, where a lower value for the cross-over distance at lower viscosity ratios was reported.[20,21] Similarly as the unit viscosity ratios, in all cases confinement seems to promote an out-of-phase breakup. In Figure 15, the results are shown for $\lambda = 4$: the cross-over distance shifts to a higher value for the higher viscosity ratio, and a higher confinement ratio shifts it back to a lower cross-over distance again. A second cross-over distance can be observed in Figure 15(b),

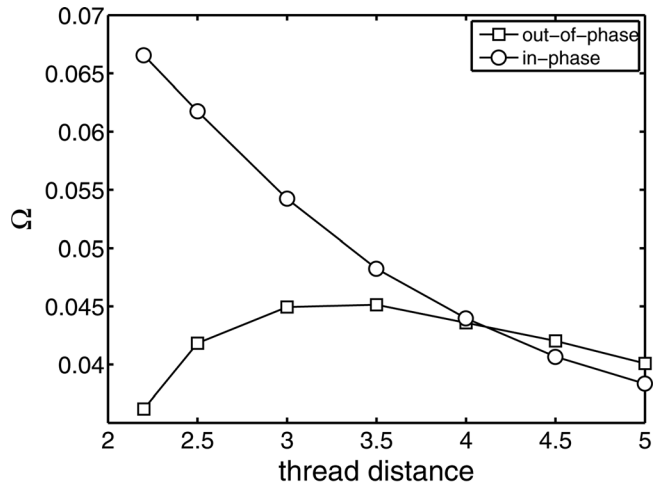

(a)

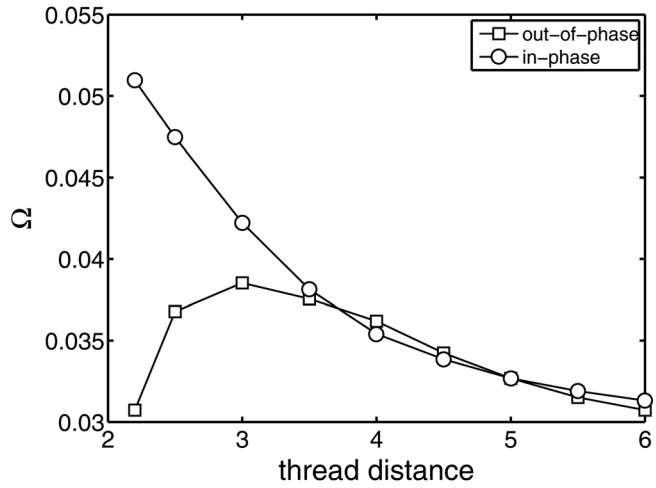

(b)

FIG. 15. As Fig. 14 for $\lambda = 4$.

which we attribute to the distance between the threads being so large that the growth speeds of the isolated threads are recovered (see Figure 6).

V. CONCLUSIONS

An algorithm to compute periodic Green's function is used to study the stability of confined threads. By comparing the growth rate of an initial sinusoidal disturbance, an excellent match is obtained with Tomotika's theory for unconfined threads. As the confinement increases, the growth rate decreases, mainly in the direction perpendicular to the walls, but overall stability is not reached, as long as the spherical thread still fits between the walls. The wave number with maximum growth speeds makes a small change, switching to lower values for $\lambda \leq 0.4$ and to higher values for $\lambda \geq 0.4$. Shear flow stabilizes the thread, as long as the capillary number is high enough. Furthermore, the interaction of multiple threads is shown. The onset of in-phase and out-of-phase breakup is reproduced. A critical thread separation of about 3 is found for unconfined threads, below which multiple threads break up in an in-phase mode, and above which the out-of-phase breakup is preferred. The critical separation shifts to smaller values for increased confinement ratios and lower viscosity ratios.

ACKNOWLEDGMENTS

This work was sponsored by the Dutch Polymer Institute (DPI), project #446. We thank K. Migler for feedback on this work and J. Blawzdziewicz and E. Wajnryb for discussing the periodic Green's functions.

[1]H. Stone, A. Stroock, and A. Ajdari, "Engineering flows in small devices: microfluidics toward a lab-on-a-chip," Annu. Rev. Fluid Mech. **36**, 381 (2004).
[2]G. Christopher and S. Anna, "Microfluidic methods for generating continuous droplet streams," J. Phys. D Appl. Phys. **40**, R319 (2007).
[3]T. Cubaud and T. Mason, "Capillary threads and viscous droplets in square microchannels," Phys. Fluids **20**, 053302 (2008).
[4]K. Humphry, A. Ajdari, A. Fernandez-Nieves, H. Stone, and D. Weitz, "Suppression of instabilities in multiphase flow by geometric confinement," Phys. Rev. E **79**, 056310 (2009).
[5]R. Suryo and O. Basaran, "Tip streaming from a liquid drop forming from a tube in a co-flowing outer fluid," Phys. Fluids **18**, 082102 (2006).
[6]S. Anna and H. Mayer, "Microscale tipstreaming in a microfluidic flow focusing device," Phys. Fluids **18**, 121512 (2006).
[7]P. Arratia, J. Gollub, and D. Durian, "Polymeric filament thinning and breakup in microchannels," Phys. Rev. E **77**, 036309 (2008).
[8]K. Migler, "String Formation in sheared polymer blends: coalescence, breakup, and finite size effects," Phys. Rev. Lett. **86**, 1023 (2001).
[9]J. Pathak, M. Davis, S. Hudson, and K. Migler, "Layered droplet microstructures in sheared emulsions: finite-size effects," J. Colloid Interface Sci. **255**, 391 (2002).
[10]J. Pathak and K. Migler, "Droplet-string deformation and stability during microconfined shear flow," Langmuir **19**, 8667 (2003).
[11]A. Vananroye, P. Van Puyvelde, and P. Moldenaers, "Structure development in confined polymer blends: steady-state shear flow and relaxation," Langmuir **22**, 2273 (2006).
[12]C. Tufano, G. Peters, and H. Meijer, "Confined flow of polymer blends," Langmuir **24**, 4494 (2008).
[13]J. Plateau, "Statique expérimentale et théorique des liquides soumis aux seules forces moléculaires," (Gauthier Villars, Paris, 1873).
[14]Lord Rayleigh, "On the capillary phenomena of jets," Proc. R. Soc. Lond. **29**, 71 (1879).
[15]S. Tomotika, "On the instability of a cyllindrical thread of a viscous fluid surrounded by another viscous fluid," Proc. R. Soc. Lond. Ser. A **146**, 322 (1935).
[16]S. Tomotika, "Breaking up of a drop of viscous liquid immersed in another viscous fluid which is extending at a uniform rate," Proc. R. Soc. Lond. Ser. A **153**, 302 (1936).
[17]H. Stone and M. Brenner, "Note on the capillary thread instability for fluids of equal viscosities," J. Fluid Mech. **318**, 373 (1996).
[18]P. Elemans, J. Janssen, and H. Meijer, "The measurement of interfacial tension in polymer/polymer systems: The breaking thread method," J. Rheol. **34**, 1311 (1990).
[19]J. Eggers, "Nonlinear dynamics and breakup of free-surface flows," Rev. Mod. Phys. **69**, 865 (1997).
[20]P. Elemans, J. van Wunnik, and R. van Dam, "Development of morphology in blends of immiscible polymers," AIChE J. **43**, 1649 (1997).
[21]Y. Knops, J. Slots, P. Elemans, and M. Bulters, "Simultaneous breakup of multiple viscous threads surrounded by viscous liquid," AIChE J. **47**, 1740 (2001).
[22]A. Gunawan, J. Molenaar, and A. van de Ven, "In-phase and out-of-phase break-up of two immersed liquid threads under influence of surface tension," Eur. J. Mech. B Fluids **21**, 399 (2002).

[23]J. Hagedorn, N. Martys, and J. Douglas, "Breakup of a fluid thread in a confined geometry: droplet-plug transition, perturbation sensitivity, and kinetic stabilization with confinement," Phys. Rev. E **69**, 056312 (2004).
[24]T. Mikami, R. Cox, and S. Mason, "Breakup of extending liquid threads," Int. J. Multiphase Flow **2**, 113 (1975).
[25]D. Khakhar and J. Ottino, "Breakup of liquid threads in linear flows," Int. J. Multiphase Flow **13**, 71 (1987).
[26]A. Frischknecht, "Stability of cylindrical domains in phase-separating binary fluids in shear flow," Phys. Rev. E **58**, 3495 (1998).
[27]A. Gunawan, J. Molenaar, and A. van de Ven, "Does shear flow stabilize an immersed thread?" Eur. J. Mech. B Fluids **24**, 379 (2005).
[28]Y. Son, N. Martys, J. Hagedorn, and K. Migler, "Suppression of capillary instability of a polymeric thread via parallel plate configuration," Macromolecules **36**, 5825 (2003).
[29]I. Bazhlekov, P. Anderson, and H. Meijer, "Numerical investigation of the effect of insoluble surfactants on drop deformation and breakup in simple shear flow," J. Colloid Interface Sci. **298**, 369 (2006).
[30]I. Bazhlekov, P. Anderson, and H. Meijer, "Non-singular boundary-integral method for deformable drops in viscous flows," Phys. Fluids **16**, 1064 (2004).
[31]J. Rallison and A. Acrivos, "A numerical study of the deformation and burst of a viscous drop in an extensional flow," J. Fluid Mech. **89**, 191 (1978).
[32]C. Pozrikidis, *Boundary-Integral and Singularity Methods for Linearized Viscous Flow* (Cambridge University Press, Cambridge, 1992).
[33]R. Jones, "Spherical particle in Poiseuille flow between planar walls," J. Chem. Phys. **121**, 483 (2004).
[34]P. Janssen and P. Anderson, "Boundary-integral method for drop deformation between parallel plates," Phys. Fluids **19**, 043602 (2007).
[35]P. Janssen and P. Anderson, "A boundary-integral model for drop deformation between two parallel plates with non-unit viscosity ratio drops," J. Comput. Phys. **227**, 8807 (2008).
[36]N. Liron and S. Mochon, "Stokes flow for a Stokes-let between 2 parallel flat plates," J. Eng. Math. **10**, 287 (1976).
[37]S. Bhattacharya, J. Bladwzdziewicz, and E. Wajnryb, "Far-field approximation for hydrodynamic interactions in parallel-wall geometry," J. Comput. Phys. **212**, 718 (2006).
[38]M. Loewenberg and E. Hinch, "Numerical simulation of concentrated emulsion in shear flow," J. Fluid Mech. **321**, 395 (1996).
[39]A. Zinchenko and R. Davis, "An efficient algorithm for hydrodynamical interaction of many deformable drops," J. Comput. Phys. **157**, 539 (2000).
[40]A. Zinchenko and R. Davis, "Shear flow of highly concentrated emulsions of deformable drops by numerical simulations," J. Fluid Mech. **455**, 21 (2002).
[41]A. Zinchenko and R. Davis, "Large-scale simulations of concentrated emulsion flows," Philos. T. Roy. Soc. A. **361**, 813 (2003).
[42]D. Frenkel and B. Smit, *Understanding Molecular Simulation: From Algorithms to Applications* (Academic, London, 2002).
[43]J. Blawzdziewicz and E. Wajnryb, "An analysis of the far-field response to external forcing of a suspension in the Stokes flow in a parallel-wall channel," Phys. Fluids **20**, 093303 (2008).
[44]A. Arnold and C. Holm, "MMM2D: a fast and accurate summation method for electrostatic interactions in 2D slab geometries," Comput. Phys. Commun. **148**, 327 (2002).
[45]N. Grønbech-Jensen, "Summation of logaritmic interactions in nonrectangular periodic media," Comput. Phys. Commun. **119**, 115 (1999).
[46]S. Ghasemi, A. Neelov, and S. Goedecker, "A particle-particle, particle-density algorithm for the calculation of electrostatic interactions of particles with slablike geometry," J. Chem. Phys. **127**, 224102 (2007).
[47]S. Tyagi, "Effective way to sum over long-range Coulomb potentials in two and three dimensions," Phys. Rev. E **70**, 066703 (2004).
[48]S. Tyagi, "Rapid evaluation of the periodic Green function in *d* dimensions," J. Phys. A: Math. Gen. **38**, 6987 (2005).
[49]A. Zinchenko, M. Rother, and R. Davis, "A novel boundary-integral algorithm for viscous interaction of deformable drops," Phys. Fluids **9**, 1493 (1997).
[50]J. Elmendorp, "A study on polymer blending microrheology," Ph.D. thesis (Delft University of Technology, The Netherlands, 1986).